

DOI: 10.21122/2220-9506-2024-15-4-323-333

Wafer-Level Packaging of Microelectromechanical Systems Based on Frame Structure

E.S. Barbin², I.V. Kulinich², T.G. Nesterenko^{1,2}, A.N. Koleda^{1,2}, E.V. Shesterikov²,
P.F. Baranov¹, D.P. Il'yaschenko¹

¹National Research Tomsk Polytechnic University,
Lenina Avenue, 30, 634050, Tomsk, Russia

²Tomsk State University of Control Systems and Radioelectronics,
Lenina Avenue, 40, 634050, Tomsk, Russia

Received 06.09.2024

Accepted for publication 14.11.2024

Abstract

Modern microelectromechanical systems (MEMS) are devices that incorporate microelectronic components and micromechanical structures on a single chip. Packaging is a mandatory stage in MEMS manufacturing. It ensures mechanical protection, sealing and transmission of electric energy and signals. The present work was aimed at developing a MEMS packaging method as a part of the consolidated manufacturing process. The method is developed on the example of a microwave MEMS switch. The switch manufacturing scheme includes conventional technologies used for producing gallium arsenide integrated circuits: optical lithography, liquid etching, electron-beam and magnetron deposition of metallic, resistive and dielectric films. The work presents a new inter-plate MEMS packaging based on a frame structure with a passivating film. The main purpose of the package frame layer is mechanical support for an upper layer of the sealing material. The frame layer should have the structure allowing for unimpeded removal of the sacrificial photoresist and be impermeable for the sealant. To satisfy the requirements stated, a metallic thin copper-film spatial frame was fabricated by galvanic deposition. The frame structure is a geodesic dome comprised of a complex network of triangle cells arranged in rows. The connected triangles create a self-supporting durable framework. The measurement and modeling results demonstrate that the round frame structure is more durable than a square frame with the same maximum cell dimensions. The stress-strain state for the round framework considerably alters depending on the number of rows of triangle cells. In addition to the mechanical support, the cell structure of the framework – with adequate selection of cell dimensions, solvent and sealant viscosities – allows for unimpeded penetration of the solvent (N-methyl-2-pyrrolidone, NMP) and removal of ma-P1225 photoresist sacrificial layers. At the same time, the layer structure is impermeable for the sealant (benzocyclobutene, BCB). The proposed MEMS switch packaging enables mass fabrication of GaAs integrated circuits in a single process, which expands their frequency range. The new plate-level packaging technology is absolutely compatible with MEMS fabrication technology without specific materials and equipment which reduces the dimensions and cost of MEMS.

Keywords: MEMS, heterointegration, packaging, geodesic dome

Адрес для переписки:

Нестеренко Т.Г.
Национальный исследовательский Томский политехнический
университет,
пр-т Ленина, 30, г. Томск 634050, Россия
e-mail: ntg@tpu.ru

Address for correspondence:

Nesterenko T.G.
National Research Tomsk Polytechnic University,
Lenin Ave., 30, Tomsk 634050, Russia
e-mail: ntg@tpu.ru

Для цитирования:

E.S. Barbin, I.V. Kulinich, T.G. Nesterenko, A.N. Koleda,
E.V. Shesterikov, P.F. Baranov, D.P. Il'yaschenko.
Wafer-Level Packaging of Microelectromechanical Systems Based
on Frame Structure.
Приборы и методы измерений.
2024. Т. 15. № 4. С. 323–333.
DOI: 10.21122/2220-9506-2024-15-4-323-333

For citation:

Barbin ES, Kulinich IV, Nesterenko TG, Koleda AN, Shesterikov EV,
Baranov PF, Il'yaschenko DP.
Wafer-Level Packaging of Microelectromechanical Systems Based
on Frame Structure.
Devices and Methods of Measurements.
2024;15(4):323–333.
DOI: 10.21122/2220-9506-2024-15-4-323-333

DOI: 10.21122/2220-9506-2024-15-4-323-333

Тонкоплёночная технология корпусирования микроэлектромеханических систем на основе каркасной структуры

Е.С. Барбин², И.В. Кулинич², Т.Г. Нестеренко^{1,2}, А.Н. Коледа^{1,2}, Е.В. Шестериков²,
П.Ф. Баранов¹, Д.П. Ильященко¹

¹Национальный исследовательский Томский политехнический университет,
пр-т Ленина, 30, г. Томск 634050, Россия

²Томский государственный университет систем управления и радиоэлектроники,
пр-т Ленина, 40, г. Томск 634050, Россия

Поступила 06.09.2024

Принята к печати 14.11.2024

Современные МЭМС – это устройства, объединяющие в себе микроэлектронные компоненты и микромеханические структуры на одном чипе. Процесс корпусирования является обязательным этапом изготовления МЭМС устройств, который обеспечивает механическую защиту, герметичное уплотнение, передачу электроэнергии и сигналов. Целью данной работы являлась разработка способа корпусирования МЭМС, который входит в единый технологический процесс изготовления устройства. Разработка такого метода корпусирования осуществлена на примере СВЧ МЭМС ключа. Схема технологического процесса изготовления СВЧ МЭМС ключа включает в себя традиционные процессы технологии арсенид-галлиевых интегральных схем, такие как оптическая литография, жидкостное травление, электронно-лучевое и магнетронное осаждение металлических, резистивных и диэлектрических плёнок. В работе представлена новая межпластинчатая упаковка МЭМС на основе каркасной конструкции с пассивирующей плёнкой. Основная задача каркасного слоя корпуса – обеспечение механической поддержки вышележащему слою герметизирующего материала. Каркасный слой должен обладать структурой, позволяющей беспрепятственно удалять жертвенный слой фоторезиста, и быть непроницаемым для герметизирующего материала. Для выполнения этих требований использована металлическая пространственная рама, выполненная на основе тонкой плёнки меди, полученной методом гальванического осаждения. Каркасная конструкция имеет форму геодезического купола, состоящего из сложной сети треугольных ячеек, расположенных рядами. Соединённые треугольники создают самоподдерживающийся структурно прочный каркас. Результаты измерений и моделирования показали, что круглая рамочная конструкция является более жёсткой, чем квадратная рамная конструкция с таким же максимальным размером ячейки. Напряженно-деформированное состояние круглой рамной конструкции существенно изменяется в зависимости от количества рядов треугольных ячеек каркасной конструкции. Кроме механической поддержки ячеистая структура каркаса при соответствующем подборе размера ячейки, вязкости растворителя и герметизирующего слоя позволяет беспрепятственно проникать растворителю (N-метилпирролидон) и удалять жертвенные слои фоторезиста ma-P1225. При этом структура данного слоя непроницаема для герметизирующего материала (бизбензоциклобутена). Предложенная упаковка МЭМС ключа позволяет серийно производить интегральные схемы GaAs, в едином технологическом процессе, что расширяет их частотный диапазон. Предлагаемая новая технология упаковки на уровне пластины полностью совместима с технологией производства МЭМС без использования специальных материалов и оборудования, что позволяет снизить габариты и стоимость МЭМС.

Ключевые слова: МЭМС, гетероинтеграция, упаковка, геодезический купол

Адрес для переписки:

Нестеренко Т.Г.
Национальный исследовательский Томский политехнический университет,
пр-т Ленина, 30, г. Томск 634050, Россия
e-mail: ntg@tpu.ru

Address for correspondence:

Nesterenko T.G.
National Research Tomsk Polytechnic University,
Lenin Ave., 30, Tomsk 634050, Russia
e-mail: ntg@tpu.ru

Для цитирования:

E.S. Barbin, I.V. Kulinich, T.G. Nesterenko, A.N. Koleda,
E.V. Shesterikov, P.F. Baranov, D.P. Il'yaschenko.
Wafer-Level Packaging of Microelectromechanical Systems Based
on Frame Structure.
Приборы и методы измерений.
2024. Т. 15. № 4. С. 323–333.
DOI: 10.21122/2220-9506-2024-15-4-323-333

For citation:

Barbin ES, Kulinich IV, Nesterenko TG, Koleda AN, Shesterikov EV,
Baranov PF, Il'yaschenko DP.
Wafer-Level Packaging of Microelectromechanical Systems Based
on Frame Structure.
Devices and Methods of Measurements.
2024;15(4):323–333.
DOI: 10.21122/2220-9506-2024-15-4-323-333

Introduction

Microelectromechanical systems (MEMS) are miniature devices with mechanical, chemical or optical sensors, integrated circuits (ICs) or photooptic integrated circuits for data management and processing. MEMS are widely used due to their small size and weight and low energy consumption, as well as lower mass production costs as compared to macrosystems. The most widely used are inertial sensors, namely MEMS gyroscopes and accelerometers [1, 2]. As of today, optical [3, 4] and radio-frequency microelectromechanical systems (RF MEMS) become increasingly popular, e. g., switched capacitors, resonators, switches, etc. [5–8].

The packaging process is compulsory for manufacturing MEMS devices, which ensures mechanical protection, hermetic sealing, transfer of electric power and signals. In addition, wafer-level packaging (WLP) must provide an appropriate price and size, be CMOS-compatible, and operate in severe conditions.

The packaging cost ranges from 30 % to 50 % of the total production cost owing to the strict requirements to packaging of brittle MEMS components [9]. The key objective for boosting microelectromechanical systems to a higher level of commercialization is to find low-cost and efficient methods of their packaging.

MEMS-packaging is performed in two ways: die-level packaging (DLP) and wafer-level packaging (WLP) [10]. The die-level packaging includes wafer dicing into several individual dies, which are consequently packaged separately or in combination with electronic and other components in a common package. The DLP process is long and expensive and requires solders or adhesives to mount MEMS dies in a package.

In the WLP process, a wafer with MEMS dies is attached to a cap wafer, which provides a sealed cavity for each die. The obtained structure is diced into individual encapsulated dies. The WLP method provides sealing of MEMS devices prior to the wafer dicing into dies and allows using standard packages of integrated circuits instead of expensive custom packages.

At present, two groups of WLP methods are used [11]. The first group utilizes eutectic and diffusion bonding of wafers and their micromachining [11–16]. The technique requires high voltage or temperature, which can damage the MEMS

structure and cause sticking of mechanically weak structures.

Temel et al. [17] proposed at eutectic bonding technique implying application of Au-Sn thin films for MEMS packaging. Au-Sn thin films were applied for the low-temperature wafer bonding using low-thickness materials. This technique eliminates the electroplating stage prior to deposition of Au-Sn thin films that are required for bonding wafers and provides less complicated and more reliable MEMS fabrication.

Low-temperature hermetic thermo-compression wafer-level bonding based on copper-electroplated sealing frame [18] provides hermetic sealing and electrical contact. It also allows for integration of micro-structured wafers. Hermetic bonding can be realized at 250 °C, when the gas formation is low, hence the pressure in the cavity is lower. Moreover, the shear bond strength exceeds 100 MPa.

The second group of WLP methods utilizes thin films to provide surface micromachining. In contrast to semiconductor wafer splicing, the thin-film encapsulation process does not require an additional wafer and provides a higher packaging density [19–23]. This technique has no restrictions on the total thickness variation (TTV) and cleanness of the wafer surface. The thin-film encapsulation process also provides electrical bonding between the circuit elements and the packaged MEMS device. The most important characteristic of this WLP method is the integration of monolithic MEMS and integrated circuits, which allows placing them in a common package, thereby improving its performance and reducing the cost.

To achieve high stability and strength of thin film packaging technology, Epi-Seal process has been developed [24, 25]. An abundant diversity of Epi-Seal-based MEMS-devices demonstrates the possibility of producing high-performance MEMS in a single production process.

At the same time, the conventional Epi-Seal process has design limitations such as maximum gap between elements of 1.5 μm , inability to implement top electrodes, etching holes should exceed 12 μm . These factors restrict the diversity of designs. Yang et al. [26] proposed a MEMS fabrication method, which eliminates the main design limitations of the conventional Epi-Seal process, its main parameters being preserved. This technique allows making gaps between elements within 0.7–50 μm and implementing both in- and out-of-plane electrodes.

Therefore, the main limitations of the MEMS packaging via wafer bonding are high wafer flatness, small total thickness variation of 1 to 10 μm , frequent wafer fracture, and a high bonding temperature of over 300 $^{\circ}\text{C}$. Thin-film packaging is the most technologically and economically justified method, since it eliminates the use of additional equipment and reduces the dimensions and mass of the end product. At the same time, the successful application of thin-film packaging for the MEMS monolithic integration requires over-coming engineering complications occurring when removing massive sacrificial layers.

According to the international roadmap, in semiconductor industry, one of the urgent tasks in IC integration with MEMS is modification and standardization of IC-technologies in conjunction with MEMS technologies [27, 28]. To simplify the process of MEMS heterointegration with ICs or PICs, the wafer-level packaging method is required that would be a part of a common technological process of MEMS fabrication.

The work is aimed at including packaging into a unified technological process of MEMS fabrication by implementing standard technological operations (lithography, liquid etching, electron-beam and magnetron deposition of metal, resistive and dielectric films). This technology will reduce dimensions and cost of MEMS devices, since they will be sealed simultaneously with their fabrication; no additional wafer and special equipment will be required (bonding). One of the solutions is implementation in MEMS fabrication of a frame structure represented by a metal geodesic dome-shaped spatial frame [29]. The dome is a spherical spatial frame structure comprised of a complex network of triangular cells

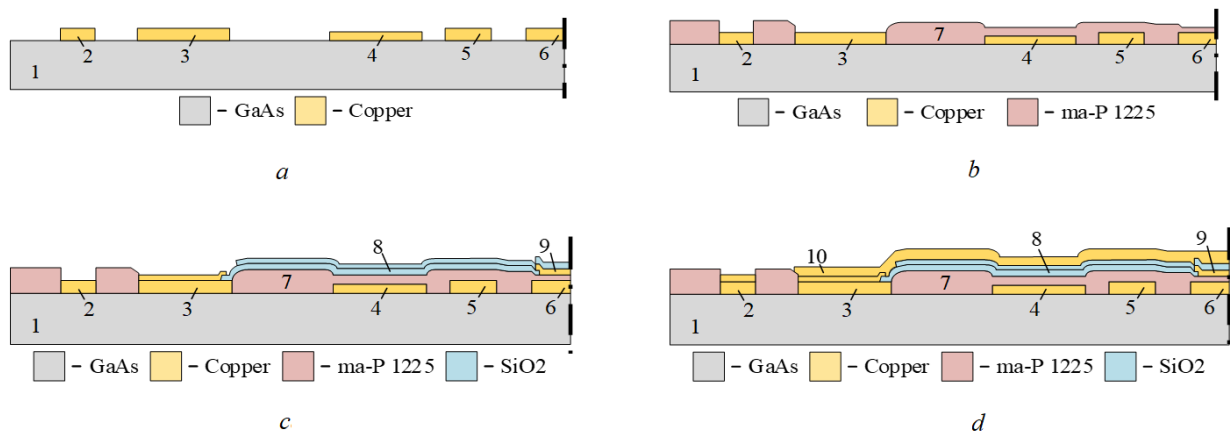
arranged in rows. The joint triangles thus create a self-supporting structurally strong frame.

In this manuscript we will present a novel technological process of MEMS wafer-level packaging based on the frame structure with a passivating layer having high mechanical strength. The developed method will provide monolithic integration of MEMS with integrated circuits based on conventional MEMS fabrication processes.

Technology process

A developed WLP, fully integrated in the process flow, is exemplified by a RF MEMS switch fabrication. The latter is intended for RF-signal switching between the elements of a monolithic IC. The RF MEMS switch is fabricated as a coplanar transmission line and consists of a signal electrode with a brake and two ground electrodes. Microwave signal switching is provided by implementing an ohmic contact in the signal line break. The ohmic contact is implemented by the gap-closing electrode placed on the cantilevered beam of the RF MEMS switch and separated from the cantilevered beam main metallization by a dielectric layer. The RF MEMS switch control is provided by two driving electrodes. There is an air gap between the cantilevered beam and driving electrodes.

Semi-insulating GaAs handle wafers with (100) crystallographic orientation were used to fabricate RF MEMS switches in a thin-film package. The flow chart is presented in Figure 1. It includes such conventional processes of the GaAs IC manufacture as optical lithography, liquid etching, electron-beam and magnetron sputtering of thin-film metals, resistive and dielectric materials.



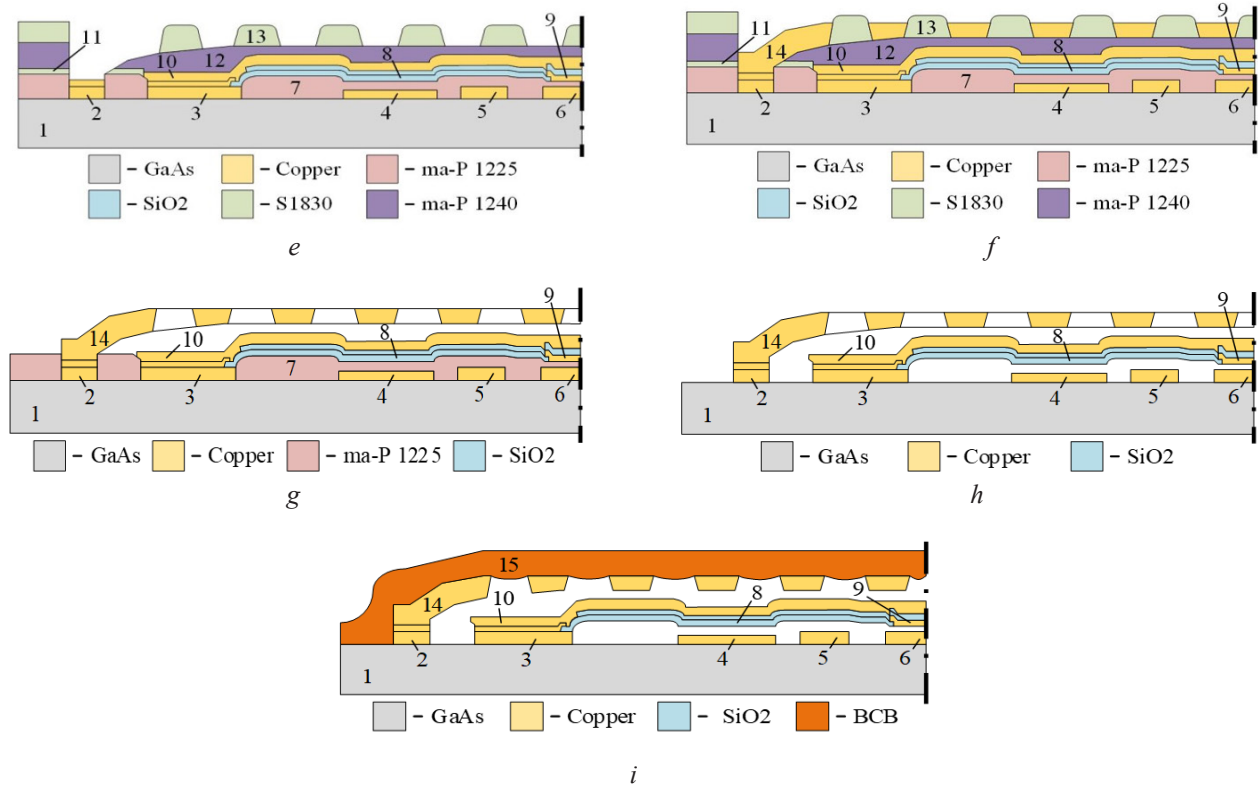


Figure 1 – Flow chart: *a* – driving electrodes, signal electrodes, cantilevered beam support of RF MEMS switch; *b* – photoresist sacrificial layer; *c* – gap-closing electrode and SiO₂ dielectric layer; *d* – cantilevered beam main metallization; *e* – RF MEMS switch structure after complete removal of photoresist sacrificial layers; *f* – frame structure plating; *g*, *h* – removal of photoresist, seed, separating, and sacrificial layers; *i* – RF MEMS switch structure in sealed package

In Figure 1 the numbers indicate: 1 – GaAs-handle wafer; 2 – frame structure anchors; 3 – cantilevered beam support; 4 – driving electrode; 5 – ground electrode; 6 – signal electrode; 7 – ma-P 1225 photoresist sacrificial layer; 8 – SiO₂ dielectric layer; 9 – gap-closing electrode; 10 – cantilevered beam main metallization; 11 – S1818 photoresist layer; 12 – ma-P 1240 photoresist sacrificial layer; 13 – S1830 photoresist masking layer for the frame structure; 14 – frame structure plating; 15 – hermetic sealing layer of benzocyclobutene (BCB). As presented in Figure 1*a*, driving, ground and signal electrodes, cantilevered beam and frame structure anchors were formed by electron beam deposition of metal films through the two layers of AZ-1518/LOR20B photoresist.

The air gap between the RF MEMS switch beam and signal electrodes was obtained by centrifugation of the 3- μ m thick ma-P 1225 photoresist sacrificial layer (Figure 1*b*). The photoresist was dried on a hot plate at 100 °C for 5 min and exposed to laser 3D-lithography on a direct write lithography system to

eliminate the thickness difference between the photoresist and signal and driving electrodes. The photoresist was developed in a tetramethylammonium hydroxide solution for 2 min.

Figure 1*c* depicts the formation of the copper film gap-closing electrode and SiO₂ separating dielectric layer using electron-beam sputtering through 2- μ m thick AZ-1518 photoresist layer with a negative slope of walls in the gap. The thicknesses of the gap-closing electrode and the dielectric layer were 300 and 200 nm, respectively. In Figure 1*d*, one can see the cantilevered beam main metallization obtained by the electroplating deposition of 2- μ m thick copper. The next stage included the frame structure formation for the RF MEMS switch packaging. It involved the deposition of the photoresist sacrificial layer and electroplating of copper for the frame structure.

Evidently from Figure 1*e*, the masking photoresist for electroplating of copper consists of ma-P1240 and S1830 photoresist sacrificial layers applied onto the RF MEMS switch beam and cantilevered beam

main metallization. The gaps were formed in the ma-P1240 photoresist sacrificial layer using laser 3D-lithography followed by the electroplating deposition of the Ti/Cu seeding layer. Next, electroplating deposition of copper was conducted through the gaps of the S1830 photoresist masking layer (Figure 1f). The copper deposition was conducted from $\text{CuSO}_4\cdot\text{H}_2\text{SO}_4\cdot\text{C}_2\text{H}_5\text{OH}$ electrolyte with a ratio of 100:70:10 g/L. At a current density of 0.1 mA/mm^2 , the copper deposition velocity was approx. $0.2 \text{ }\mu\text{m/min}$. The specific resistance of the obtained film was $0.021 \text{ }\mu\text{Ohm m}$.

Photoresist masking, seeding, separating, and sacrificial layers were removed after the frame structure electroplating (Figure 1g, h). The copper-plated separating and seeding layers were removed by liquid etching in $\text{HCl}:\text{H}_2\text{O}:\text{FeCl}_3$ (1:10:1) solution. $\text{NH}_4\text{F}:\text{HCl}:\text{H}_2\text{O}$ (1.5:100:10) solution was used for Ti thin film etching. These etchants demonstrate high selectivity during the etching process. Photoresist masking layers were removed by N-Methylpyrrolidone (NMP) followed by washing in isopropyl alcohol and drying with nitrogen. The drying and examination of the sacrificial layers and the wafer were followed by the ultimate stage (Figure 1i). The spin coating of $7\text{-}\mu\text{m}$ thick BCB on the frame structure provided the sealing of the RF MEMS switch. Then, we used photolithography to disclose the contact grounds of the RF MEMS switch. The coated BCB sealing layer was then dried at $250 \text{ }^\circ\text{C}$ for 20 min. The fabricated sealed RF MEMS switch structure is presented in Figure 1i.

We should note that on the packaging of all the elements on the wafer, the hardening occurs after the formation of the street, which causes no global warping of the plate.

Modeling

Several samples of the following type were used for The main purpose of the package frame layer is mechanical support of the upper layer of the sealing material. Moreover, the frame layer should possess the structure that would allow unhindered removal of the sacrificial photoresist layer. Consequently, the layer structure should be impenetrable for the sealant. The combination of such properties can be achieved by using a spatial frame from electroplated thin copper film. The frame structure was built as a geodesic dome comprised of several rows of triangular cells. The variations of the frame structure geometry are presented in Figure 2.

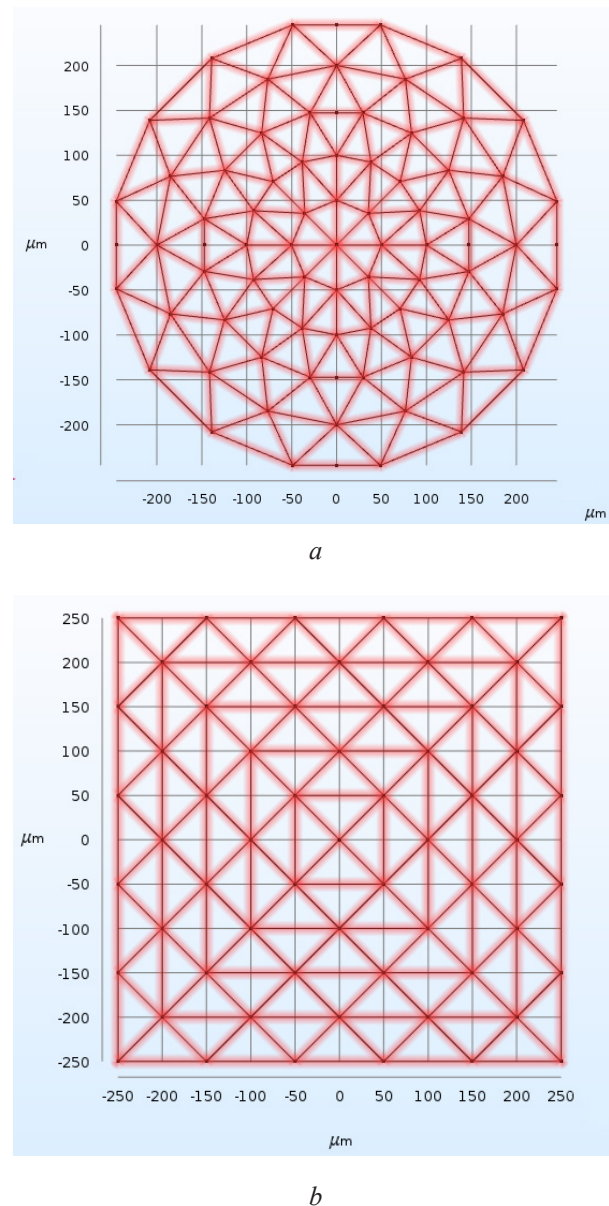


Figure 2 – Round (a) and square (b) geometries of the frame structure

Geodesic domes conventionally have round base (Figure 2a), so they experience less stresses. For the sake of comparison, we considered a frame with a square base (Figure 2b). The frame structure was researched using a finite element method (FEM) in the COMSOL. The frame structure was attached to the outer perimeter of the structure. When designing the structure and defining its geometric parameter, the applied load was equal to the BCB-layer with a thickness of $5 \text{ }\mu\text{m}$ multiplied by a coefficient 1.7 at normal conditions which accounts for additional stresses due to the shrinkage and BCB-layer thickness error. The modeled layer thickness is $8.5 \text{ }\mu\text{m}$.

Afterwards, due to the hardening of the BCB-layer, it becomes self-supporting. As a result, the structure strength increases due to the metallic frame and self-supporting BCB-layer.

The height of the frame structure at its maximum point was determined by the thickness of the photoresist sacrificial layer. The thickness of sacrificial layer between of RF-switch and frame structure is 8 μm . Obviously from Figure 3, the round frame structure is more rigid than the square frame structure having the same maximum cell size.

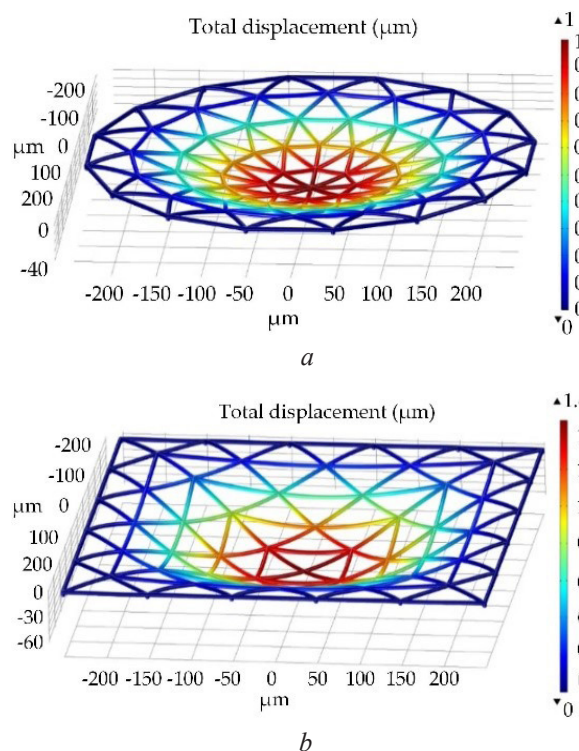


Figure 3 – Stress and deformation of round (a) and square (b) frame structure

The FEM was used to model the stress-strain state of the round frame structure with varying numbers of rows of triangular cells (Figure 4).

As presented in Figure 4, the stress-strain state of the round frame structure significantly changes depending on the number of the rows of triangular cells in the frame structure. Frame structures with 5 or more rows are acceptable because the stress in structure does not exceed a yield strength for copper of 70 MPa. For frame structure of 5 rows of triangular cells maximum deformation under the applied loads equal no more than 0.2 μm and frame structure will not contact the RF MEMS switch. In addition to the mechanical support, the frame structure configuration must provide free NMP

penetration to remove the ma-P1240 photoresist sacrificial layers. At the same time, the frame structure must be impermeable to the BCB sealing material. The cellular frame structure can satisfy these requirements by an appropriate selection of the cell size, viscosity of the remover and sealing layer. The optimal size of the triangular cell of the frame structure should be selected by mathematical simulation.

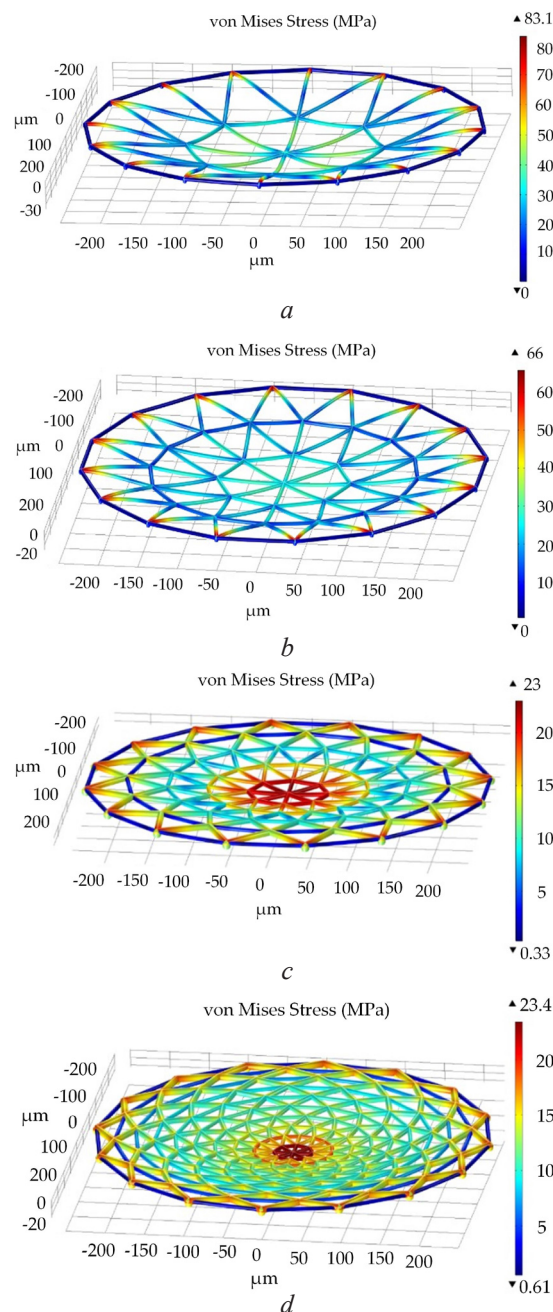


Figure 4 – Stress analysis of the frame structure depending on the number of rows of triangular cells. a – 2 rows of triangular cells; b – 3 rows of triangular cells; c – 5 rows of triangular cells; d – 10 rows of triangular cells

Figure 5 presents a 2D-model of an elementary frame structure element which shows penetration of BCB into the frame structure. Figure 5a shows

the simulation result of the distribution of BCB fractions and air fractions after BCB layer coating on the framework layer.

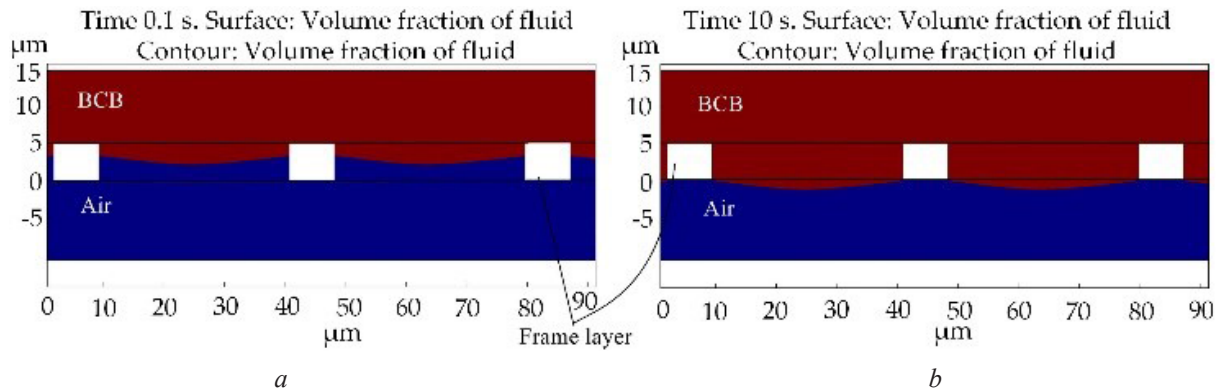


Figure 5 – Distribution of benzocyclobutene – fractions and air fractions on the framework layer: *a* – result after 0.1 s; *b* – result after 10 s

Starting from 0.1 s (Figure 5a), there is an evident penetration of BCB into the frame structure. After 10 s (Figure 5b), the penetration of BCB stabilizes; there is no penetration under the dome due to surface tension of BCB. Therefore, BCB fills the frame cells, but cannot reach the RF-switch structure. Figure 6 depicts the simulation of NMP penetration through the frame structure for sacrificial layer removal.

crograph in Figure 7 presents the RF MEMS switch packaging fabricated by this technology. Figure 7a corresponds to the technological step in Figure 1h.

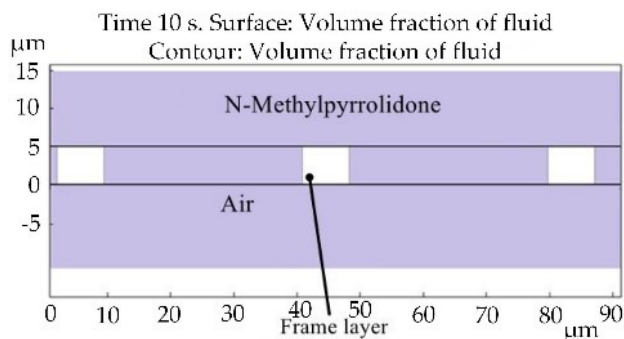


Figure 6 – Volume fractions of remover and air after 10 s of remover deposition

Figure 6 present the moment of time (10 s after) when the NMP completely penetrated under the frame structure and substituted air. Therefore, the optimal cell size at which NMP penetrates with non-penetrating BCB equals 30 μm . The optimal size of a triangular cell is the maximum gap that equals the median of an isosceles triangle of the cell itself.

The mathematical simulation shows that the selected frame configuration meets the requirements for the package frame structure and can be used to remove the photoresist sacrificial layers followed by the RF MEMS switch packaging. The photomi-

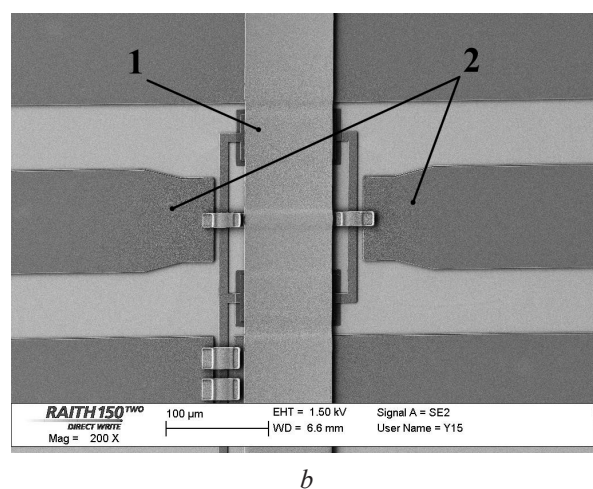
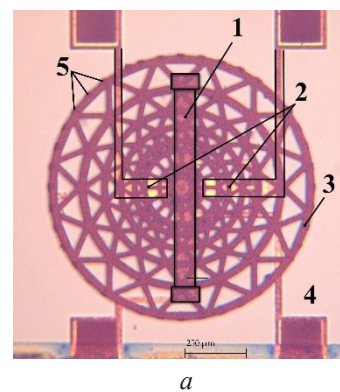


Figure 7 – Photomicrograph of the RF MEMS switch packaging: *a* – with frame structure; *b* – without frame structure; 1 – cantilevered beam; 2 – signal line; 3 – frame structure; 4 – driving electrode; 5 – anchors

Figure 8 shows the frame structure with sacrificial layer of ma-P 1240.

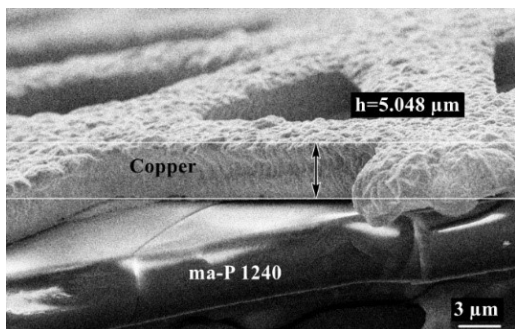


Figure 8 – The frame structure with sacrificial layer of ma-P 1240

After the removal of the seeding and sacrificial layers, the frame structure is hermetized (for liquid) by the BCB layer and the gaps in the BCB layer are opened to provide an access to the electrical contacts of the RF MEMS switch. The scattering parameters of the RF MEMS switch obtained before and after its packaging are presented in Figure 9.

According to Figure 9, the RF MEMS switch parameters decrease by 6.1 dB in the on state, while in the off state, they increase by 4.9 dB. This is explained by the wave reflection from the three-dimensional metal frame structure.

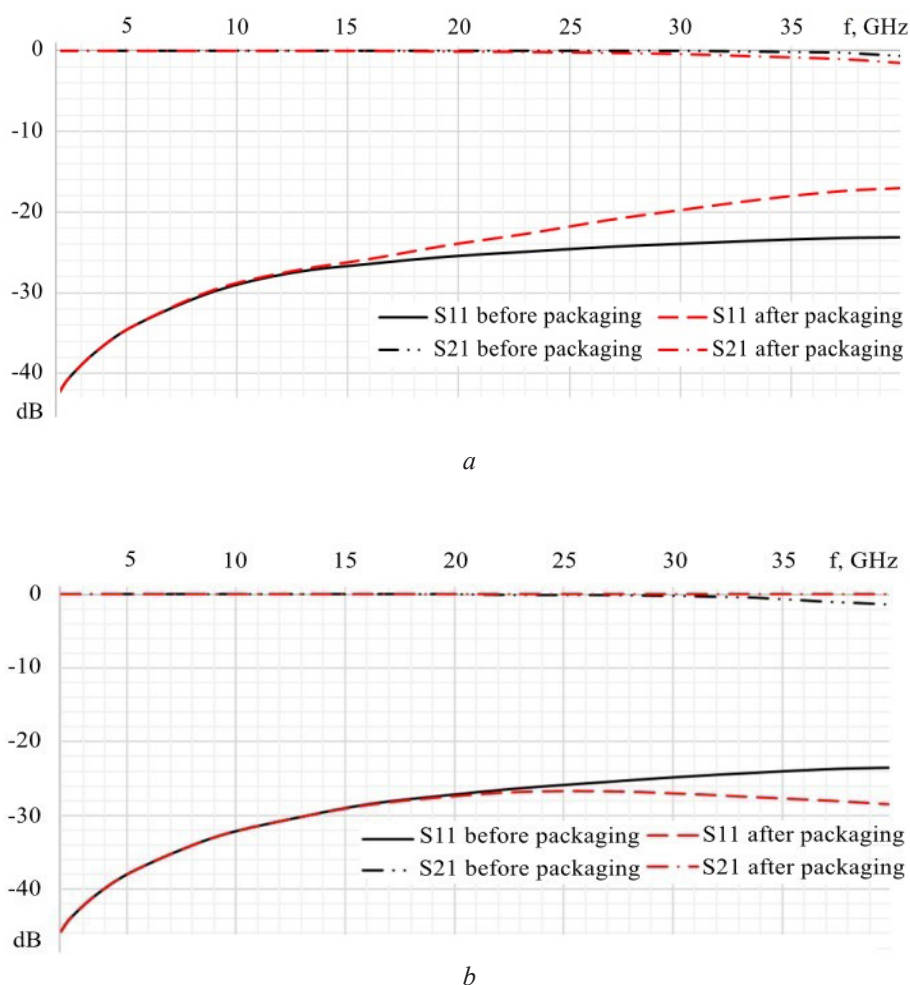


Figure 9 – S-parameters of the RF MEMS switch: a – on state; b – off state

The following parameters were obtained for the RF MEMS switch: average contact resistance of 2.46 Ohm on a semiconductor wafer; switch-on time of 80 μs; control voltage of 25 V.

Conclusion

The proposed novel wafer-level packaging technique is completely compatible with the MEMS

production technology without the use of specific materials and equipment. The use of the three-dimensional metal frame structure as a mechanical support for the frame structure allowed fully removing the photoresist sacrificial layers with the successive RF MEMS switch packaging.

The proposed RF MEMS switch packaging allows serial production of GaAs integrated circuits, including radio frequency switches, in a single technological process, which widens the frequency range of GaAs RF integrated circuits. The comparative analysis showed that the proposed RF MEMS switch fabrication implementing electroplating deposition of copper can compete with its rivals based on the electroplating deposition of gold. The presented techniques were used to achieve the high performance of the RF MEMS switch and can also be applied in the production of high-resolution MEMS sensors, such as gyroscopes, accelerometers, high-quality resonators and hybrid optical MEMS. Evidently from the comparative analysis of various crystal packaging technologies such as wafer-level packaging and die-level packaging, the technology suggested by us is cheaper and simpler, since it requires no additional evacuation equipment.

Acknowledgments

The results were obtained within the state assignment of the Ministry of Science and Higher Education of the Russian Federation (theme no. FEWM-2024-0008).

References

1. Xia D, Yu C, Kong L. The Development of Micro-machined Gyroscope Structure and Circuitry Technology. *Sensors*. 2014;14(1):1394-1473. **DOI:** 10.3390/s140101394
2. Xie H, Fedder GK. Fabrication, Characterization, and Analysis of a DRIE CMOS-MEMS Gyroscope. *IEEE Sensors Journal*. 2003;3(5):622-631. **DOI:** 10.1109/JSEN.2003.817901
3. Olsson RH, Bogart GR, Baker MS, Carr DW, Swiler TP, Clews PJ, Krishnamoorthya U. In-plane MEMS-based nano-g accelerometer with sub-wavelength optical resonant sensor. *Sensors and Actuators A: Physical*. 2008:283-290 pp. **DOI:** 10.1016/j.sna.2008.03.017
4. Samuelson SR, Xie HA. Large Piston Displacement MEMS Mirror with Electrothermal Ladder Actuator Arrays for Ultra-Low Tilt Applications. *Journal of Microelectromechanical Systems*. 2014;23(1):39-49. **DOI:** 10.1109/JMEMS.2013.2290994
5. Zhang H, Huang J, Yuan W, Chang HA. High-Sensitivity Micromechanical Electrometer Based on Mode Localization of Two Degree-of-Freedom Weakly Coupled Resonators. *Journal of Microelectromechanical Systems*. 2016;25(5):937-946. **DOI:** 10.1109/JMEMS.2016.2598780
6. Pillai G, Zope AA, Tsai JM, Li S. Design and Optimization of SHF Composite FBAR Resonators. *IEEE Transactions on Ultrasonics, Ferroelectrics, and Frequency*. 2017;64(12):1864-1873. **DOI:** 10.1109/tuffc.2017.2759811
7. Li SS, Lin YW, Xie Y, Ren Z, Nguyen CT. Micromechanical hollow-disk ring resonators. *Proceedings of the IEEE International Conference on Micro Electro Mechanical Systems*. 2004:821-824 pp. **DOI:** 10.1109/MEMS.2004.1290711
8. Lee J E-Y, Yan J, Seshia AA. Study of lateral mode SOI-MEMS resonators for reduced anchor loss. *Journal of Microelectromechanical Systems*. 2011;21(4):1-10. **DOI:** 10.1088/0960-1317/21/4/045010
9. Lawes LA. Manufacturing costs for microsystems/MEMS using high aspect ratio microfabrication techniques. *Microsystem Technologies*. 2006;13(1):85-95. **DOI:** 10.1007/s00542-006-0252-6
10. Beeby S, Ensel G, Kraft M, White N. *MEMS Mechanical Sensors*. 2004, Publisher: Artech House, Boston, London, 269 p.
11. Tilli M, Motooka T, Airaksinen V, Franssila S, Paulasto-Kröckel M, Lindroos V. *Handbook of Silicon Based MEMS Materials and Technologies*. 2015, Edition: 2nd, Publisher: Elsevier, 800 p.
12. Zhang M, Yang J, He Y, Yang F, Yang F, Han G, Ning J. Research on a 3D Encapsulation Technique for Capacitive MEMS Sensors Based on Through Silicon Via. *Sensors*. 2019;19(1):93. **DOI:** 10.3390/s19010093
13. Xu P, Si C, He Y, Wei Z, Jia L, Han G, Ning J, Yang F. A Novel High-Q Dual-Mass MEMS Tuning Fork Gyroscope Based on 3D Wafer-Level Packaging. *Sensors*. 2021;21(19). **DOI:** 10.3390/s21196428
14. Torunbalci MM, Gavcar HD, Yesil F, Alper SE, Akin T. An all-silicon process platform for wafer-level vacuum packaged MEMS devices. *IEEE Sensors Journal*. 2021;21(13). **DOI:** 10.1109/JSEN.2021.3073928
15. Moriyama M, Suzuki Y, Kumano M, Totsu K, Hirano H, Tanaka S. Metal-bonding-based hermetic wafer-level MEMS packaging technology using in-plane feedthrough: Hermeticity and high frequency characteristics of thick gold film feed-through. *IEEE Transactions on Sensors and Micromachines*. 2019;38(10). **DOI:** 10.1541/ieejsmas.138.485
16. Nesterenko TG, Barbin ES, Koleda AN, Baranov PF, Tanaka S, Tsukamoto TA. Novel multiple-axis MEMS

gyro-scope-accelerometer with decoupling frames. *Sensor Review*. 2019;39(5):670-681.

DOI: 10.1108/SR-05-2018-0133

17. Temel O, Kalay YE, Akin T. Wafer-Level Low-Temperature Solid-Liquid Inter-Diffusion Bonding With Thin Au-Sn Layers for MEMS Encapsulation. *Journal of microelectromechanical systems*. 2021;30(1):64-71.

DOI: 10.1109/JMEMS.2020.3040039

18. Farisi MS Al, Hirano H, Tanaka S. Low-temperature hermetic thermo-compression bonding using electroplated copper sealing frame planarized by fly-cutting for wafer-level MEMS packaging. *Sensors and Actuators A: Physical*. 2018;279:671-679.

DOI: 10.1016/j.sna.2018.06.021

19. Zhang Q, Cicek P-V, Nabki F, El-Gamal M. Thin-film encapsulation technology for above-IC MEMS wafer-level packaging. *Journal of micromechanics and microengineering*. 2013;23(12):1-10.

DOI: 10.1088/0960-1317/23/12/125012

20. He R, Kim C-J. On-Wafer monolithic encapsulation by surface micromachining with porous polysilicon shell. *Journal of Micromechanical Systems*. 2007;16(2):462-472. **DOI:** 10.1109/jmems.2007.892797

21. Verheijden GJAM, Koops GEJ, Phan KL, JTM van Beek. Wafer-level encapsulation technology for MEMS devices using an HF permeable PECVD SIOC capping layer. *IEEE 21st International Conference on Micro Electro mechanical systems*. 2008:798-801 p.

DOI: 10.1109/MEMSYS.2008.4443777

22. Lee BK, Choi DH. Use of nanoporous columnar thin film in the wafer-level packaging of MEMS devices. *Journal of Micro-mechanics and Microengineering*. 2010;(20):20-29. **DOI:** 10.1088/0960-1317/20/4/045002

23. Rajaraman V, Pakula LS, Pham HTM, Sarro PM, French PJ. Robust wafer-level thin-film encapsulation of micro-structures using low stress PECVD silicon carbide. *IEEE 22nd International Conference on Micro Electro mechanical systems*. 2009:140-143 p.

DOI: 10.1109/MEMSYS.2009.4805338

24. Candler RN, Park Woo-Tae, Li Huimou, Yama G, Partridge A, Lutz M, Kenny TW. Single wafer encapsulation of MEMS devices. *IEEE Transactions on Advanced Packaging*. 2003;26(3):227-232.

DOI: 10.1109/TADVP.2003.818062

25. Ng EJ, Lee HK, Ahn CH, Melamud R, Kenny TW. Stability of silicon microelectromechanical systems resonant thermometers. *IEEE Sensors Journal*. 2013;13(3):987-993.

DOI: 10.1109/JSEN.2012.2227708

26. Yang Y, Ng EJ, Chen Y, Flader IB, Kenny TW, Hong VA. A Unified Epi-Seal Process for Fabrication of High-Stability Microelectromechanical Devices. *Journal of Microelectromechanical Systems*. 2016;25(3):489-497.

DOI: 10.1109/JMEMS.2016.2537829

27. International Technology Roadmap for Semiconductors (ITRS). Micro-Electro-Mechanical Systems (MEMS) Summary. Available online: <https://www.semiconductors.org/wp-content/uploads/2018/08/2013MEMS.pdf> (accessed on 10 April 2022).

28. Qu H. CMOS MEMS Fabrication Technologies and Devices. *Micromachines*. 2016;7(1):14.

DOI: 10.3390/mi7010014

29. Geodesic Domes and Space-Frame Structures, Available online: <https://www.thoughtco.com/what-is-a-geodesic-dome-177713> (accessed on 10 may 2022).